A periplasmic cupredoxin with a green CuT1.5 center is involved in bacterial copper tolerance

Anne Durand, Mélanie Fouesnard, Marie-Line Bourbon, Anne-Soisig Steunou, Elisabeth Lojou, Pierre Dorlet, Soufian Ouchane

A periplasmic cupredoxin with a green CuT1.5 center is involved in bacterial copper tolerance.

Anne Durand[1#], Mélanie Fouesnard[1], Marie-Line Bourbon[1], Anne-Soisig Steunou[1], Elisabeth Lojou[2], Pierre Dorlet[2#] and Soufian Ouchane[1#]

[1] Université Paris-Saclay, CEA, CNRS, Institute for Integrative Biology of the Cell (I2BC), 91198 Gif-sur-Yvette, France. [2] CNRS, Aix Marseille Université, BIP, IMM, Marseille, France.

Correspondence: soufian.ouchane@i2bc.paris-saclay.fr, anne.durand@i2bc.paris-saclay.fr, Phone: (33)-169823137 and to pdorlet@imm.cnrs.fr Phone: (33)-491164414.

Running title: A green CuT1.5 type protein involved in copper tolerance.

Keywords: copper, toxicity, metalloprotein, green type cupredoxin, periplasm, EPR.

Abstract

Importance of copper resistance pathways in pathogenic bacteria is now well recognized since macrophages use copper to fight bacterial infections. Additionally, considering the increase of antibiotic resistance, growing attention is given to the antimicrobial properties of copper. It is of primary importance to understand how bacteria deal with copper. The Cu resistant cuproprotein CopI is present in many Human bacterial pathogens and environmental bacteria and crucial under microaerobiosis (conditions for most pathogens to thrive within their host). Hence, understanding its mechanism of function is essential. CopI proteins share conserved histidine, cysteine and methionine residues that could be ligands for different copper binding sites among which acupredoxin center that could be involved in the protein function. Here, we demonstrated that, *Vibrio cholerae* and *Pseudomonas aeruginosa* CopI restore Cu resistance phenotype in *Rubrivivax (R.) gelatinosus ΔcopI* mutant. We identified that Cys^{125} (ligand in the cupredoxin center) and conserved histidines and methionines are essential for *R. gelatinosus* CopI (*Rg*CopI) function. We also performed spectroscopic analyses of the purified *Rg*CopI protein and showed that it is a green cupredoxin able to bind a maximum of three Cu(II) ions: (i) a green Cu site (CuT1.5), (ii) a type 2 Cu binding site (T2) located in the N-terminal region, (iii) a third site with a yet unidentified location. CopI is therefore one member of the poorly described CuT1.5 center cupredoxin family. It is unique, since it is a single domain cupredoxin with more than one Cu site involved in Cu resistance.

Graphical Abstract

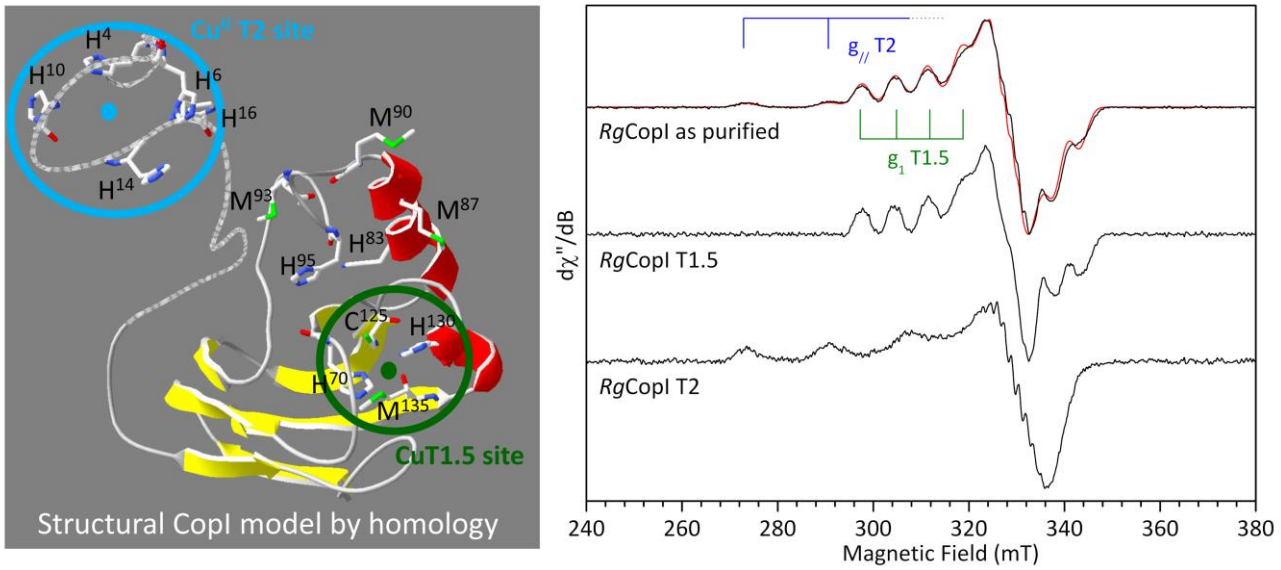

Introduction

Copper (Cu) is present in many enzymes involved in metabolisms like respiration or photosynthesis. Although essential, Cu can be cytotoxic even at low concentrations. Cu toxicity is part of the innate immune response [1] and Cu-resistance mechanisms are thus important for the virulence of human bacterial pathogens [2-4]. Therefore, a tight control of Cu cellular level is vital and bacteria rely on various Cu homeostasis mechanisms to deal with Cu excess. Moreover, there is an increased interest in antimicrobial copper properties (Cu-compounds, Cu-based surfaces and nanoparticles…) to deal with antibiotics and multidrug resistance [5]. Understanding Cu homeostasis is therefore highly relevant, since it could also provide valuable targets for novel antibacterial drugs, as recently reported for the Cu export system [6]. Most known cuproproteins are located in the bacterial envelope, therefore an efficient Cu homeostasis system is required in this compartment to protect cells form Cu toxicity and to provide Cu cofactor to fulfil protein function. The well-conserved Cu-efflux ATPase CopA translocates Cu(I) from the cytoplasm to the periplasm where Cu(I) can be sequestered, oxidized or expelled outside the cells [7]. Various periplasmic proteins involved in Cu handling were identified in many Gram negative bacteria and they display different activities to detoxify Cu(I) [2, 8-14]. Their diversity highlights their essential role to protect cells from the highly toxic Cu(I). However, the mechanisms by which most of these proteins contribute to Cu tolerance is not yet well known. The *Escherichia (E.) coli* Cu tolerance system is the best characterized [7]. Under aerobiosis, the multicopper oxidase (MCO) CueO oxidizes Cu(I) into the less toxic Cu(II) in the periplasm [15, 16]. Under anaerobiosis CueO is inactive and Cu(I) is exported across the outer membrane through the CusCBA efflux system [17]. CueO and Cus are not conserved among all bacteria and other systems protect the periplasm and the membranes from Cu toxicity. Cu(I) is more toxic than Cu(II) and it is the major form under anaerobiosis and microaerobiosis. Handling Cu(I) is thus crucial for bacteria living under low oxygen conditions, such as various Human bacterial pathogens and environmental bacteria. Nonetheless, only few examples of periplasmic cuproproteins required under anaerobiosis were reported. Recently, the *Pseudomonas* (*P.) aeruginosa* CopG protein, with a thioredoxin domain, was proposed to oxidize Cu(I) and its role in Cu resistance under anaerobiosis was highlighted [11]. Moreover, disruption of *PA2807* (*copI* homologue) in *P. aeruginosa* led to a Cu sensitive phenotype [13, 18]. In the Human intestine pathogen *Vibrio (V.) cholerae,* CopG and Cot were respectively proven to be involved in Cu resistance under aerobic and anaerobic conditions or only under aerobiosis [19]. In the photosynthetic bacterium *Rubrivivax (R.) gelatinosus*, the cupredoxin CopI is important for Cu resistance under low oxygen or anaerobic photosynthetic growth condition [20]. Under the same

conditions, *R. gelatinosus* CopJ (a protein with a CxCC motif and a thioredoxin-like domain as in CopG) is also induced by Cu [20]. CopI and CopJ are homologues to *V. cholerae* Cot and CopG respectively. In the photosynthetic bacterium *Rhodobacter capsulatus*, the MCOs CutO and CopG are involved in Cu resistance under anaerobiosis [21, 22]. In other bacteria, strong induction of mRNA and/or proteins homologous to CopI under excess Cu was reported [13, 14, 23], suggesting a key role of CopI in Cu homeostasis.

Cupredoxins are a major class of redox-active metalloproteins, with high electron transfer efficiencies, commonly found in biological systems [24]. Single-domain cupredoxins (10-20 kDa) possess a mononuclear type 1 Cu site (CuT1), which gives rise to particular spectroscopic, structural and redox properties. Two nitrogens from two histidines, a sulfur from a cysteine and usually a sulfur from a methionine coordinate the Cu atom at the T1 site. Based on their Cu center geometry, the cupredoxins were classified into the blue type (azurin, plastocyanin) [25], the green type also called CuT1.5 (three are currently described: *Acidithiobacillus (A.) ferrooxidans* AcoP [26], auracyanin [27] and copper nitrite reductase [28]) and the red type (*Nitrosomonas europeae* nitrosocyanin [29]). The *R. gelatinosus* CopI, *V. cholerae* Cot and *P. aeruginosa* PA2807 are predicted to be single-domain cupredoxins with a CuT1 center [13, 19, 20]. Interestingly, in comparison with single-domain cupredoxins (plastocyanin or azurin), they display additional sequences bearing putative Cu-binding residues (methionines and histidines). How CopI detoxify Cu(I) under anaerobiosis or microaerobiosis in bacteria deserves further studies given that most pathogens thrive under oxygen-limited conditions within their host. In this context, we show here that expression of *V. cholerae* Cot or *P. aeruginosa* PA2807 in *R. gelatinosus ΔcopI* mutant restores anaerobic growth in the presence of Cu. These data contrast with previous work where Cot was not required in *V. cholerae* for Cu resistance under anaerobic conditions [19]; however the role of *P. aeruginosa* PA2807 in copper resistance was not tested previously under anaerobic conditions [13, 18]. Therefore, CopI, Cot and PA2807 belong to the same bacterial protein family and fulfil the same function. CopI protein was spectroscopically characterized as purified from *R. gelatinosus* and Cu(II) binding was studied since Cu(I) is EPR silent. Moreover, under our conditions, total Cu quantification showed that there is no Cu(I) bound to the purified protein. Additionally, biophysical characterization of CopI purified from *R. gelatinosus* and mutagenesis studies identified two Cu(II) binding sites and revealed that the predicted "blue copper" CopI is rather a "green copper" type cupredoxin. Based on our overall findings, we present a model for CopI function to detoxify periplasmic Cu as a working hypothesis for further studies.

Materials and Methods

Bacterial strains, growth and growth inhibition: E. coli and *V. cholerae* were grown at 37°C in LB medium. *R. gelatinosus* was grown at 30°C (unless otherwise described), aerobically, microaerobically (*e.g*. 250 mL flasks filled with 250 mL medium) or anaerobically under light (photosynthesis in filled and sealed tubes) in malate growth medium. Anaerobic growth on plates was performed using Anaerocult P. bags (Merck). Kanamycin was added at 50 µg/mL and tetracycline at 1 µg/mL. The malate medium copper concentration is 1.6 µM and $CuSO_4$ was added at different concentrations. Bacterial strains and plasmids are listed in TABLE SI. For growth inhibition, cells were grown overnight, diluted 1:100 in the same medium with indicated $CuSO_4$ concentrations and incubated overnight under anaerobic photosynthesis. OD^{600nm} for *V. cholerae* or OD^{680nm} for *R. gelatinosus* was measured after overnight growth using the Tecan Infinite M200 luminometer (Tecan, Mannerdorf, Switzerland).

For soluble protein preparation, cells were grown semi-aerobically in 0.25 L of malate medium in a 0.5 L flask) in the presence of 1 mM $CuSO_4$ to induce the protein expression. Cells were incubated at 30°C (180 RPM) until the $OD^{680\ nm}$ reaches a value between 0.6 to 1. Bacteria were centrifuged at 4,000 *g* for 15 min at 4°C, pellets were washed twice with 40 mL of sodium phosphate buffer 0.1 M pH 7.5, then frozen in liquid nitrogen and stored at -80°C.

Molecular biology techniques: Standard methods were performed according to Sambrook *et al.* [30]. WT and mutated *copI* genes were produced by the DNA synthesis services (GENEWIZ and Genscript). All constructs were under the Cu inducible *copA* promoter in pUC57-Km and were sub-cloned in the expression vector pBBR1MCS-3. For *V. cholerae copI* (*VCA0261-0260*), the wild type gene including its own sequence encoding the signal peptide was used. In contrast, for *P. aeruginosa copI* (*PA2807*), the native sequence encoding the signal peptide was substituted by *R. gelatinosus* CopI signal peptide and the N-terminus His-rich sequence to allow respectively the periplasmic localization and the detection. The resulting plasmids (Table SI) were introduced into *R. gelatinosus ΔcopI* mutant by electroporation as previously described [31]. Transformants were selected on malate plates supplemented with the appropriate antibiotics under aerobiosis.

Soluble protein preparation: Bacterial cell pellets were resuspended in 0.05 M sodium phosphate buffer (pH 7.5) to reach an OD^{680nm}/mL of 7 to perform cell lysis by sonication. After sonication, two centrifugations were performed: a first run at 11,000 *g* for 20 min at 4°C followed by a 208,000 *g* for 2h00 at 4°C. The supernatant (soluble fraction) containing CopI

proteins was recovered and concentrated 25 to 50 times depending on the sample on an YM-10 (Millipore) concentrator. Glycerol (5% v/v) was then added, the fraction was frozen in liquid nitrogen and stored at -20°C. Protein concentrations were determined using the bicinchoninic acid assay (Sigma) with bovine serum albumin as a standard.

SDS-PAGE and Western blot: Equal amount of disrupted cells (1 OD^{680nm}) heated 10 min at 95°C were separated on SDS-PAGE (14% polyacrylamide) and transferred onto a Hybond ECL Polyvinylidene difluoride membrane (GE Healthcare). Membrane was then probed with the HisProbe-HRP (horseradish peroxidase, Pierce) according to the manufacturer's instruction. Bands were revealed using a chemiluminescent HRP substrate according to the method of Haan and Behrmann [32]. Image capture was performed with a ChemiDoc camera system (Biorad).

Protein purification: WT CopI protein was purified from *R. gelatinous* WT cells grown microaerobically (2 L) for 48 h at 30°C with shaking at 190 rpm and in the presence of 1.2 mM $CuSO_4$. Cells were pelleted by centrifugation at 3,000 *g* for 15 min at 4°C. The bacterial pellet was washed with 30 mL of phosphate buffer 0.1 M pH 7.5 and centrifuged as before. For cell lysis by sonication, the bacterial pellet was resuspended to reach an $OD^{680\ nm}$/mL around 9 in a phosphate buffer 20 mM, NaCl 500 mM pH 8.0, supplemented with cOmplete™, Mini EDTA-free Protease Inhibitor Cocktail Roche and DNAse 50 µg/mL. Lysed cells were then centrifuged at 12,000 *g* for 20 min at 4°C. The resulting supernatant was centrifuged at 208,000 *g* for 1h30 at 4°C. The soluble fraction was then loaded on a CuIMAC preequilibrated with sodium phosphate 20 mM, NaCl 0.5 M pH 8.0 buffer, elution was performed in the same buffer with increasing imidazole concentrations from 0 to 50 mM followed by two steps at 50 and 250 mM imidazole. Eluted fraction containing CopI protein was then loaded on a gel filtration chromatography (see below).

The $CopI^{5His}$ protein was purified from a periplasmic enriched fraction obtained from 1 L culture of microaerobically grown *R. gelatinosus* cells expressing $CopI^{5His}$ (48 h culture) in the presence of 1.2 mM $CuSO_4$. The periplasm was extracted using a freeze/thaw method according to [33]. While the $CopI^{2His}$ protein was purified from a 0.5 L culture of semi-aerobically (0.5 L of culture in a 1 L flask) grown *R. gelatinosus* cells expressing $CopI^{2His}$ (24 h culture at 37°C) in the presence of 1 mM $CuSO_4$. The periplasmic enriched fraction containing the $CopI^{2His}$ protein was obtained after resuspending the bacterial pellet at an $OD^{600\ nm}$ of 6 U/mL in a Tris/HCl 50 mM pH 8.0, EDTA 1 mM, saccharose 0.45 M, lysozyme 5 mg/mL. The resuspended cells were

incubated for 1h at 30°C with shaking at 100 RPM and centrifuged at 12,000 *g* for 15 min at 4°C. CopI^{5His} and CopI^{2His} were purified according to the same purification protocol. The enriched periplasmic fraction was ultracentrifuged (208,000 *g* for 1h30 at 4°C) and the supernatant was differentially precipitated (40-60% ammonium sulfate). The pellet recovered from the 60% ammonium sulfate precipitation was resuspended in HEPES 50 mM pH 8.0 and desalted using a PD10 column or dialysis. The resulting sample was loaded onto a 5 mL CM FF HiTrap column, elution was performed using a linear gradient of NaCl (5 column volumes from 0 to 250 mM NaCl) in HEPES 50 mM pH 8.0 buffer. The fraction of interest was then directly loaded on a CuIMAC column equilibrated with HEPES 50 mM pH 8.0 buffer for CopI^{5His} protein or with 2.5 mM imidazole, NaCl 500 mM, HEPES 50 mM pH 8.0 buffer for CopI^{2His} protein. For CopI^{5His}, the protein of interest was collected in the flow-through fraction. For CopI^{2His} protein, the elution was performed applying a linear gradient of 12 column volumes from 2.5 to 100 mM imidazole in NaCl 500 mM HEPES 50 mM pH 8.0 buffer. The CopI^{2His} protein eluted at around 40 mM imidazole (similarly to the WT protein). For both proteins, the collected fraction was then loaded on a gel filtration chromatography (see below).

For the three purifications described above, all the chromatographic steps were performed using an AKTA purifier system and the absorbance at three wavelengths was recorded (280, 439 and 581 nm; the latter two wavelengths are characteristics of the CuT1 centre). The last chromatographic step is a gel filtration performed identically; except that a Superdex 200 HiLoad 16/60 column was used for WT CopI, while a Superdex 75 HiLoad 16/600 was used for the two mutant proteins. Briefly, the sample was concentrated on an Amicon YM-10 (Millipore) before loading and the column was performed in phosphate 50 mM pH 7.5 buffer with NaCl 0.15 M. The fraction of interest collected was concentrated and frozen in liquid nitrogen before storage at -80°C in the presence of glycerol 5% (v/v). Throughout the purification steps, the protein was followed by Coomassie-stained SDS-PAGE and Western blot, but for the CopI^{5His} protein the Western blot was not performed since the five histidines responsible of the signal were mutated. The purity of the protein was estimated by Coomassie blue-stained SDS-PAGE. The protein concentration of the pure proteins was determined by measuring the absorbance at 280 nm using the extinction molar coefficient of 6,990 M^{-1}. cm^{-1} based on the composition of the protein sequence and assuming the binding of Cu does not affect it significantly. For all measurements on purified proteins the buffer was sodium phosphate 50 mM, NaCl 0.15 M pH 7.5 buffer unless otherwise stated.

Optical absorption spectroscopy: Absorption spectra were obtained on a single beam Cary 60 Spectrophotometer. The baseline was recorded against a buffer sample (sodium phosphate 50 mM, NaCl 0.15 M pH 7.5) and automatically subtracted from all spectra.

ICP-MS: Quantification of total copper present in pure CopI was performed by high resolution ICP-MS (MasSpecLab, University of Versailles, France). Pure WT CopI (100 µM) and a control of buffer were treated identically. Sample (50 µL) was diluted 4 times in deionized water and 25 µL of internal standard containing 0.8 µL of Gallium was added. Nitric acid (200 µL) was added and the mixture was placed in quartz tubes. Samples were then mineralized with a microwaves Ultrawave (Milestone, Sorisole, Italy) under a pressure of 40 bars. They were then diluted to 6 mL with deionized water and analysed on an ICP-MS high resolution Element XR (Thermofisher, les Ulis, France) spectrometer. A calibration curve was performed in parallel.

EPR spectroscopy: EPR spectra were recorded on a Bruker Elexsys 500 spectrometer equipped with a continuous flow Oxford Instruments ESR 900 cryostat. 10% glycerol was used in the buffer (NaPi 50 mM pH 7.4, NaCl 150 mM; unless otherwise stated) for frozen samples. Simulations were performed by using the Easyspin toolbox [34] and routines locally written. Isotropic N superhyperfine coupling was taken into account for the simulations as well as g- and A- strains.

To determine the total amount of copper ions in the purified protein, EPR spectra were recorded on the purified protein sample before and after its treatment with hydrochloric acid (releasing the full Cu content of the protein into the buffer under the Cu(II) form). The double integration of the EPR spectra allowed the determination of the Cu(II) concentration by using a calibration curve obtained by recording the EPR spectra of aqueous copper sulphate solutions of variable known concentrations.

Cyclic voltammetry: Cyclic voltammetry (CV) was performed at 25°C in a standard 3-electrode cell using a potentiostat from Eg&G instrument (model 263A) controlled by Echem software. AgCl/Ag and Pt-wire were used as reference and auxiliary electrodes, respectively. All potentials are quoted *vs* NHE (normal hydrogen electrode) reference electrode by adding 210 mV to the measured potential. In a typical experiment, 2 µL of 50 µM protein in 10 mM bisTris buffer pH 7.0 was entrapped between the surface of a pyrolytic graphite electrode (surface =

0.07 cm^2) and a dialysis membrane of appropriate cut-off. This design allows to work under thin layer configuration [35]. Midpoint potentials E_m were calculated by the average of anodic and cathodic potential peaks E_p.

Homology modelling: The three-dimensional model of *Rg*CopI was built using the homology modelling suite Modeller (v10.1) with the following multi-templates: plastocyanins (pdb codes: 1JXD, 1KDJ, 1PND), azurin (pdb code: 1NWP), auracyanins (pdb codes: 1OV8, 1QHQ, 2AAN, 6KOL, 6L9S). The cupredoxin Cu was included in the alignment for rebuilding the CopI model. The multiple sequence alignment (**Fig. S1**) used as input for Modeller was generated using Jalview 2.10.5 with ClustalW algorithm and refined by manual adjustment. A run of 500 models was performed and the generated models sorted by the Modeller objective function were evaluated by their DOPE (Discrete Optimized Protein Energy) and GA341 scores calculated by Modeller. The best models corresponding to the lowest DOPE score were submitted to the QMEAN scoring function server (https://swissmodel.expasy.org/qmean/) for model quality assessment. The final model retained had a DOPE score of -11577 and a normalized QMEAN score of 0.65. The views were generated with Swiss-PDB viewer program.

Results

Sequence analyses and homology modelling revealed conserved residues within CopI

Sequence alignments of CopI from various species (**Fig. 1**) as well as with cupredoxins (**Fig. S1**) suggest the presence of a conserved type 1 (T1) Cu site and two conserved sequences with histidines and methionines, putatively involved in Cu binding in CopI. Interestingly, these latter two sequences are absent in single domain blue type cupredoxins (azurin or plastocyanin) (**Fig. S1**). Therefore, they could be important for the function of CopI. A possible structure of *Rg*CopI was obtained by homology modelling using various structures of T1 Cu proteins as templates (auracyanin, azurin and plastocyanin). This model suggests a core structure having a classic cupredoxin-fold: a sandwich with seven β strands, and two helices, α1 between β4 and β5 and α2 between β6 and β7. The T1 Cu site is not surface exposed and it involves His^{70}-Cys^{125}-His^{130}-Met^{135}. The latter three residues are conserved in the C-terminus sequence of the analyzed proteins and they are located in a loop between strands β6 and β7. While His^{70} is located in a loop between strands β3 and β4, it is identified as the fourth Cu ligand based on homology modelling and sequence alignments. These four residues are conserved in all reported

sequences (**Fig. 1**). A second sequence, referred to as internal His/Met-rich sequence, is also present in all CopI homologues. In particular, this sequence contains conserved histidines (*Rg*CopI: His^{83} His^{95}) and methionines (*Rg*CopI: Met^{87} Met^{90}) suggesting a role for these residues in CopI function. In the model structure, His^{83} and Met^{87} are located in the helix α1, while Met^{90}, Met^{93} and His^{95} are in an unfolded loop. Other less conserved histidines and methionines are present in this sequence. They vary among species with only one in *Rg*CopI (Met^{93}) and with the highest abundance in *Pseudomonas* (*P. aeruginosa*: 8 methionines and 3 histidines). The third sequence is the N-terminus His-rich or His/Met-rich sequence. It has numerous histidines (5 in *Rg*CopI) or it contains both histidines and methionines (4 His/9 Met in *Vc*Cot = *Vc*CopI). Interestingly, this sequence is absent in CopI sequences of *Pseudomonas* species (**Fig. 1A**) and it might be compensated by their longer His/Met-rich sequence. Both internal and N-terminus His/Met-rich sequences are absent in the cupredoxins used as templates for homology modelling (**Fig. S1**). Consequently, the N-terminus is unstructured in our model and strand β1 starts at Val^{35}. Interestingly, homology modelling of *Rg*CopI structure revealed the proximity of the Cu T1 site to residues of the internal His/Met-rich sequence. His^{95} and Met^{87} are 6-10 Å apart of Cu T1 site (**Fig. 1B**). Since histidines, methionines and cysteines are common Cu ligands, their conservation within CopI suggests a role in Cu binding and in its function, both investigated thereafter.

V. cholerae and *P. aeruginosa* CopI homologues protect the periplasm from Cu

Previous *in silico* analyses indicated that the periplasmic CopI is present in many bacteria but absent in *E. coli* [20]. In particular, CopI homologues were identified in bacterial pathogens such as Cot in *V. cholerae*, VS_II0517 in *Vibrio (V.) tasmaniensis*, PA2807 in *P. aeruginosa* and CinA in *P. putida* [13, 18, 19, 36]. These proteins share conserved histidines, cysteine and methionine that could form a T1 Cu center. Interestingly, they also have His- or His/Met-rich sequences that could be involved in Cu binding and in the protein function (**Fig. 1A**). The role of CopI towards Cu tolerance in some of these bacteria was suggested by their increased expression in response to Cu excess [13, 14, 18, 23, 36]. In contrast, disruption of *cot* in *V. cholerae* generated Cu susceptibility only under aerobiosis [19]. The absence of a Cu sensitive phenotype in the *V. cholerae cot* disrupted strain under anaerobiosis [19], and the moderate Cu sensitive phenotype in the *PA2807* (*copI* homologue) disrupted strain of *P. aeruginosa* [13, 18] could be presumably due to the presence of other detoxification systems. Since, *R. gelatinosus ΔcopI* mutant is highly sensitive to Cu under microaerobiosis or

anaerobiosis, we used this attractive host to test Cu tolerance function of Cot and PA2807. Heterologous expression of Cot (or *Vc*CopI) and *Rg*PA2807 (PA2807 with the N-terminus His-rich sequence of *R. gelatinosus* CopI (**Fig. S2**)) rescued the growth defect of the *ΔcopI* mutant under anaerobiosis in the presence of $CuSO_4$ (**Fig. 2**). We assume that the N-terminus His-rich sequence of *Rg*CopI added to PA2807 does not contribute to the observed phenotype, since the five histidines of this sequence are not required for Cu resistance in *Rg*CopI (see below). Additionally, the substitution of the N-terminus His-rich sequence of *Rg*CopI by the N-terminus His/Met-rich sequence of *Vc*CopI (**Fig. S2**) does not affect the Cu resistance phenotype, since the *VcRg*CopI construct behaves similarly to *Rg*CopI (**Fig. 2**). Altogether, the sequence homologies, the high Cu induction of these proteins in the WT strains and the present complementation tests are consistent with a direct role for *Vc*CopI and PA2807 in Cu tolerance under anaerobiosis. We suggest that these two proteins function similarly to *Rg*CopI. We thus propose to rename PA2807 into *P. aeruginosa* CopI (*Pa*CopI) and *V. cholerae* Cot into *Vc*CopI.

CopI expression in *R. gelatinosus* and *V. cholerae* is higher under low oxygen concentration conditions

In *R. gelatinosus*, CopI is required under Cu stress, mainly under anaerobic photosynthesis or microaerobic respiration [20]. In contrast, in *V. cholerae*, *Vc*CopI was reported to be required under aerobiosis, while its expression seems to be increased both under aerobiosis and anaerobiosis conditions under Cu stress [19]. To have a better insight into the expression profile of both *Rg*CopI and *Vc*CopI in response to oxygen and increasing $CuSO_4$ concentrations, the amount of CopI protein was assessed in both species grown under these conditions. Both proteins can be detected on Western blot by conventional His-probe, thanks to the presence of His-rich sequences. *Rg*CopI was only induced by increasing $CuSO_4$ concentrations under microaerobic respiration or photosynthesis (**Fig. 3A**). However, it was not detected under aerobiosis even at high copper concentrations (1 mM $CuSO_4$). In *V. cholerae* WT, CopI is expressed under both oxygen conditions, the amount increasing with increasing $CuSO_4$ concentration (**Fig. 3B**). Nevertheless, under low copper stress (100 to 500 µM $CuSO_4$), *Vc*CopI amount is much lower under aerobiosis than under microaerobiosis, as it was previously reported [19]. Despite the higher expression level of *Vc*CopI under anaerobiosis in comparison with aerobiosis, *Vc*CopI was shown to be important for Cu tolerance only under aerobiosis in *V. cholerae* [19]. Yet, here we showed that *Vc*CopI restored a Cu resistance phenotype in a *R. gelatinosus ΔcopI* mutant under anaerobic conditions (**Fig. 2**). This protein is therefore functional

under oxygen-limited conditions, but in *V. cholerae* another protein(s) is (are) likely responsible for Cu resistance under anaerobiosis. Overall, CopI expression is copper dependent, but its expression is also subject to oxygen concentration and/or regulation. CopI expression is better enhanced by copper under hypoxic conditions than in aerobiosis both in *R. gelatinosus* and *V. cholerae*.

Biophysical characterization of the copper binding sites of *R. gelatinosus* CopI

We took advantage of the high level of *Rg*CopI expression in WT *R. gelatinosus* cells grown under Cu excess in microaerobiosis to purify the protein and to perform its biophysical characterization as purified. Two chromatographic steps (CuIMAC and a gel filtration) were sufficient to purify *Rg*CopI at a high level of purity (**Fig. S3**) and with an average yield of 10 mg pure *Rg*CopI/L of culture. The purified protein is monomeric (15 kDa) (**Fig. S3**). ICP-MS analysis of the pure protein suggested that *Rg*CopI binds at least two Cu ions per protein since a ratio of 1.2 Cu atoms/*Rg*CopI was measured. The pure protein solution has a dark green color (**Fig. 4** inset) similar to AcoP [26] and not the typical blue color of plastocyanin or azurin.

The absorption spectrum of the purified *Rg*CopI protein (**Fig. 4**, purple) showed three main peaks at 447 nm, 582 nm and around 720 nm similar to the spectrum reported for the green type AcoP [26]. They are attributed to a S(Cys)→Cu σ charge-transfer, a S(Cys)→Cu π charge transfer and a d-d transition, respectively [37]. The R_L value (ratio between the absorbance of 447 and 582 nm peaks) for oxidized *Rg*CopI is 1.1 which classifies *Rg*CopI in the poorly described type 1.5 cupredoxin (green type) category like AcoP (R_L of 1.3). It is clearly different from the well characterized blue type 1 cupredoxins (R_L<1) [26]. Addition of $CuSO_4$ to the protein did not significantly affect the bands at 582 and 720 nm (**Fig. 4)**. However, above two equivalent of copper per protein a new band is resolved around 328 nm and the band at 447 nm shifted to a lower wavelength (438 nm). The band at 328 nm is compatible with a His to Cu LMCT and could be appearing already above one equivalent of copper per protein although it is hard to distinguish. This suggests the presence of a third Cu(II) site in the protein.

EPR is a method of choice to characterize Cu(II) binding sites in proteins. The EPR spectrum of the purified CopI protein from *R. gelatinosus* is reported in **figure 5A** (black trace, top spectrum). The amount of Cu(II) can be determined by EPR by doubly integrating the spectrum and comparison with results from a standard titration curve. The result gives around 1.1-1.2 Cu(II)/protein in agreement with the ICP-MS data. In addition, treatment of the sample with hydrochloric acid releases all the Cu content into the buffer under the Cu(II) form. The amount of

Cu after acidic treatment is equal to the amount of Cu(II) before acidic treatment. All the Cu in the purified protein is therefore under the Cu(II) redox state and there is no Cu(I) present. This amount varies slightly from one purification to another but more than one Cu(II) per protein is always observed. Qualitatively, the spectra are composed of two contributions indicating that CopI has at least two Cu(II) binding sites. From the low field portion of the spectra, it appears that one Cu(II) has a high $g_{//}$-value and significant hyperfine coupling in that direction while the other has a lower value compatible with what has been observed for cupredoxins. Quantitative analysis has been performed by simulation of the spectra (**Fig. 5A**, red trace). It was also possible to isolate the signatures of both contributions (**Fig. 5A** and see below). The relevant parameters are given in TABLE 1 along with parameters from other comparable Cu(II) sites (full parameters for the simulations are given in TABLE SII). EPR spectroscopy confirms the presence of a green Cu cupredoxin binding site, with parameters close to those observed in AcoP or NiR. For this site, the coordination sphere is composed of two nitrogen and two sulfur atoms provided by two histidines, a methionine and a cysteine. In addition, a second and more conventional, square planar Cu(II) binding site is observed. Using the Peisach-Blumberg empirical correlation [38] and in comparison with other systems, we can suggest a three nitrogen one oxygen (3N1O) equatorial binding mode for the T2 site in *Rg*CopI, although it is not possible to fully exclude a 4N coordination. Since the quantification of copper per protein showed that both sites were not fully loaded, we performed a titration of purified *Rg*CopI by addition of Cu(II) from a copper sulfate solution followed by EPR (**Fig. 5B**). The purified protein contains a little over 1 equivalent of Cu(II). The first additions of Cu(II) induced a significant increase in the relative intensity of the T2 contribution, showing that it is the site most depleted during protein purification. After the addition of one equivalent of Cu(II), we can consider that both sites are fully loaded (2 Cu(II) per protein), yet the EPR signal keeps increasing in intensity with Cu(II) addition till about two equivalents of Cu(II) are added (a total of 3 Cu(II) per protein). After that, the intensity of the EPR signal is stable, the extra copper added precipitates in the pH 7.5 buffer and it is not detected by EPR. The signal of the fully loaded protein is quite broad and the different contributions cannot be distinguished. This is most likely due to the overlap of the signals and the broadening of their line shapes because of spin-spin interaction between the Cu(II) ions. In line with what was observed with UV-visible spectroscopy, we can conclude that *Rg*CopI is able to bind a maximum of 3 Cu(II) ions and that the third site is close enough to the other two to broaden the EPR lineshape of the individual signals. At this stage, we cannot isolate the EPR signature of the third site nor conclude about its possible geometry and ligands. By contrast, using the first EPR spectra of the Cu titration allowed isolating the signatures of the T1.5 and T2 sites (**Fig. 5A**).

The midpoint redox potential of the T1.5 copper center of pure *Rg*CopI was probed by cyclic voltammetry. The cyclovoltammogram obtained at pH 7.0, shows a quasi-reversible wave at E_m = 0.31 V/NHE (ΔEp = 240mV) (**Fig. 6**). Experiments performed at pH 6.0 (**Fig. S4**) led to a more reversible wave (ΔEp = 90mV) with a similar E_m = 0.33 V/NHE, however. This potential is consistent with green cupredoxin centers and therefore the wave was attributed to the T1.5 Cu site of *Rg*CopI. No other redox event, that could be in particular linked to the second site, was observed under our experimental conditions.

Copper coordinating ligands of the three putative Cu sites and characterization of the respective mutants in *Rg*CopI

To identify the residues involved in the three putative Cu binding sites (CuT1, N-terminus His-rich and internal His/Met-rich sequences) and their role in Cu tolerance, we generated mutants of these three sites in *Rg*CopI (TABLE SIII). Strains harboring the mutated genes were tested for *in vivo* Cu resistance and their EPR spectra were also characterized.

As mentioned previously, *Rg*CopI possesses conserved residues of a CuT1.5 center (His^{70}, Cys^{125}, His^{130} and Met^{135}). In the CuT1.5 center, Cu is tightly bound thanks to the strong ligands provided by the thiolate sulfur of the cysteine and the imidazole nitrogens from the two histidines. Mutation of this cysteine is usually enough to break this interaction and lead to a complete loss of the T1.5 Cu. To probe the involvement of this center in *Rg*CopI function, we generated *Rg*$CopI^{C125S}$, a protein in which the Cys^{125} was substituted by a serine. The $CopI^{C125S}$ protein was produced albeit in lower amounts than the WT (**Fig. S5**), but it failed to restore the Cu tolerance in the complemented strain (**Fig. 7**), demonstrating a role of Cys^{125} in the CopI function. The His-rich N-terminus and the highly conserved histidines and methionines present in the internal His/Met sequence within CopI are good candidates to be involved in the second copper binding site revealed by the ICP-MS and the EPR analyses. To test this hypothesis, we constructed (i) two mutated proteins of the internal His/Met sequence ($CopI^{2His}$ and $CopI^{3Met}$, with His^{83} and His^{95} or Met^{87}, Met^{90} and Met^{93} mutated respectively), and (ii) one mutated protein of the His-rich N-terminus ($CopI^{5His}$, with His^4 His^6 His^{10} His^{14} His^{16} mutated). Substitution of the two histidines and the three methionines also failed to rescue the phenotype of *ΔcopI* mutant under Cu stress (**Fig. 7**). The corresponding proteins were detectable in all complemented strain albeit in lower amounts than the WT for $CopI^{2His}$ (**Fig. S5**). Surprisingly, mutation of the five histidines within the N-terminus, did not affect the activity of the protein, since the $CopI^{5His}$ mutant exhibited a WT Cu resistance phenotype (**Fig. 7**). These data clearly attest for the key role

of Cys^{125}, the two histidines and three methionines within the internal His/Met sequence in the Cu resistance function of CopI, while the five histidines in the N-terminus are non-essential for this function.

We also recorded EPR spectra for the mutated proteins (**Fig. 8**). Due to difficulties in the production and further purification of several mutated proteins, we first studied bacterial soluble fractions. Unfortunately, a significant type 2 Cu signal due to another endogenous copper protein was present in the control (*ΔcopI* strain transformed with empty plasmid). It impaired the analysis with respect to the presence of the CopI T2 site (**Fig. 8A**). However, the control soluble fraction did not show any cupredoxin signal, while the T1.5 signal was observed for the WT soluble fraction. Therefore, CopI was the only protein in the soluble fraction to exhibit a cupredoxin center. Furthermore, the $CopI^{5His}$ and $CopI^{3Met}$ proteins also exhibited a clear T1.5 contribution as the WT. However, the EPR spectrum of $CopI^{2His}$ and $CopI^{C125S}$ soluble fractions is largely dominated by the additional type 2 signal and it did not allow concluding on the presence or not of the CuT1.5 site. The $CopI^{2His}$ and $CopI^{5His}$ proteins were then purified and their EPR spectra were recorded (**Fig. 8B**) to unambiguously identify the Cu T1.5 site and to determine whether the T2 site was coordinated by the histidines from the internal His/Met-rich sequence or from the N-terminal sequence. The T1.5 contribution is clearly seen in both cases. A small contribution from a type 2 signal is also visible, but given the very low protein concentration, any small Cu contamination could be responsible for this. To discriminate whether this signal corresponded to the T2 signal of the native protein or not, we compared the evolution of the signal upon addition of Cu(II) ions to the $CopI^{2His}$ and $CopI^{5His}$ proteins with the WT protein complemented with Cu. For the $CopI^{2His}$, the spectrum (**Fig. 8B**) looks like that obtained for the WT protein (**Fig. 5B**, red spectrum). On the contrary, the added Cu(II) to the $CopI^{5His}$ leads to a different spectrum, which is similar to that obtained by adding Cu(II) to the Tris buffer, thus indicating that the extra Cu goes rather into the buffer. Based on these observations, the 5His mutation seems to have a bigger effect, in contrast with the 2His mutation; this strongly suggests that the T2 site is located in the N-terminus sequence of the protein and involves some of the five histidines.

Discussion

CopI is a new member of the green cupredoxin family. The *Rg*CopI T1.5 site has EPR parameters similar to those of other green cupredoxins such as AcoP and nitrite reductase (NiR), in clear contrast with typically axial EPR spectra observed for blue type cupredoxins (TABLE 1). The UV-visible and electrochemical data also fit with a green type cupredoxin. CopI is therefore a

new example of the few known members of the T1.5 cupredoxin family. Despite the absence of structure, the excellent conservation of the specific cupredoxin ligands in the sequence alignment allows proposing His^{70}, Cys^{125}, His^{130} and Met^{135} as the ligands of the Cu ion in the T1.5 site of *Rg*CopI. This CuT1.5 site is essential for CopI function. We should emphasize that care should be taken with annotated genomes since CopI proteins are incorrectly annotated "Blue copper proteins". So far, sequence differences do not allow to differentiate between green or blue types of CuT1 sites. Therefore, without a spectroscopic analysis these proteins should be named "Type 1 Cu proteins or Cupredoxins" without specifying their color.

By contrast to single domain cupredoxins characterized to date, purified CopI exhibits a second Cu(II) site. The EPR spectrum of CopI is reminiscent of that of green Cu NiR [39, 40]. Indeed, green NiR displays both T1.5 and T2 sites but they are located in two different domains of the protein. In addition, the T2 site of NiR has tetrahedral geometry with three histidine ligands and a water molecule [41], whereas the CopI T2 site has a conventional square planar geometry. The binding of nitrite to NiR T2 significantly affects its EPR spectrum [40], whereas the spectrum of CopI with added nitrite remains essentially unchanged (**Fig. S6**). This suggests that there is no open position in the equatorial plane of this site in *Rg*CopI and that the ligands are all provided by the protein amino acids and not a solvent molecule for example. It also disfavors a NiR function for the CopI protein. Interestingly, the EPR parameters of the CopI T2 site are quite similar to those determined for the low pH form of the Cu-amyloid β complex [42]. Moreover, the similarity in the N-terminus sequences of *Rg*CopI and Cu-amyloid β complex is remarkable, since the first two amino acids (aspartate and alanine) are identical and since histidines are present a bit further along. These first two amino acids are critical for Cu(II) binding to amyloid β [42] and the same type of binding mode could apply to *Rg*CopI. This suggests that the localization of the T2 site is in the His-rich N-terminus of *Rg*CopI, in full agreement with the results obtained here on *Rg*CopI mutants.

The presence of CopI in various bacteria including pathogens imposes understanding its mechanism of action. We report in the current work the functional and spectroscopic characterization of CopI, a new member of the green cupredoxin family involved in bacterial Cu resistance. We propose that CopI proteins constitute a unique subfamily of cupredoxins. Although the molecular mechanism of Cu detoxification remains to be elucidated, the presence of three Cu binding sites including a CuT1.5 site suggests that CopI proteins have an unprecedented mechanism to detoxify periplasmic Cu. Cu(I) oxidation is one of the periplasmic Cu detoxification process. Multicopper oxidases, such as copper efflux oxidase CueO, perform this reaction and they have a mononuclear type 1 Cu center (T1) acting in electron transfer to a

trinuclear Cu center (TNC) where dioxygen is reduced [43]. CueO and CopI are markedly different. CopI is smaller in size, it has no TNC and it is crucial under low oxygen conditions. CueO couples the Cu(I) oxidation to O_2 reduction, while CopI is probably unable to perform this reaction. Therefore, CopI should have a different and new mechanism to detoxify Cu. We propose that CopI binds Cu(I), methionines and/or histidines of the internal His/Met sequence being potentially involved in such Cu(I) binding, then Cu(I) could be oxidized by the redox active CuT1.5 site. An external electron acceptor (such as the putative thioredoxin CopJ) could recycle the Cu(I) of the CuT1.5 site. Finally, Cu(II) could be sequestered by the His-rich N-terminus (CuT2 site identified by EPR) similarly to the proposed function of the His-rich C-terminus of the *Mycobacterium tuberculosis* GroEL1 [44, 45]. *Rg*CopI His^{83} and His^{95} in the internal His/Met sequence are highly conserved, but they are not ligands of the CuT2 site. Interestingly, in the 3D structure model, they are close to the CuT1 site (**Fig. 1**). In this putative model, the first two steps (Cu(I) binding and oxidation) are essential since $CopI^{2His}$, $CopI^{3Met}$ and $CopI^{C125S}$ mutants are sensitive to Cu. On the contrary, the Cu(II) sequestration step would not be essential for Cu detoxification, since the $CopI^{5His}$ mutant displays a WT Cu resistance phenotype. The absence of the conserved N-terminus in *Pseudomonas* species CopI (**Fig. 1**) argues for a non-essential role of this sequence. According to our data, the Cu T2 site is coordinated by 3N and 1O in *Rg*CopI and this Cu site is lost in the $CopI^{5His}$ mutant. Therefore, a maximum of three out of the five histidines in the N-terminus could be ligands of Cu(II). Since the $–NH_2$ terminus is also a strong candidate for N ligand, it is likely that only two histidines participate in Cu binding. This putative mechanism is proposed based on our current data. It requires further investigation and will be used as working hypothesis. Among others, studies on Cu(I) binding to CopI are underway in our laboratories. For example, whether the 3rd Cu(II) site is a weak Cu(II) site or a primary Cu(I) site will be further investigated. In addition, Cu(I) oxidation by CopI in the presence or not of potential partner proteins (see below) will need to be addressed.

Our current work opens new relevant questions to complete the understanding of CopI function. The most striking difference between *R. gelatinosus* and *Vibrio* CopI proteins is a longer N-terminus highly rich in methionines (9 in *V. cholerae*, 15 in *V. tasmaniensis*, none in *R. gelatinosus*) in addition to various histidines (from 4 to 6) (**Fig. 1**). Since methionines can be Cu ligands, it raises the question whether and how they participate in *Vibrio* species CopI function. Spectroscopic analysis identified a third Cu(II) site, but its ligands and its physiological relevance are to be proven, although histidines of the N-terminus or of the internal His/Met sequence could be ligands of this third Cu atom. In *P. aeruginosa*, CopI is important for Cu resistance, nonetheless, this study was performed only under aerobiosis [13, 18]. In *V. cholerae*, CopI is

involved in Cu resistance under aerobiosis but not under anaerobiosis [19], although CopI is highly induced under anaerobiosis [19] and microaerobiosis (**Fig. 3B**). A putative partner of CopI is CopJ (CopG in *V. cholerae* and *P. aeruginosa*). In *V. cholerae*, CopG is important for Cu resistance under anaerobiosis [19], while in *P. aeruginosa* CopG is expressed under both aerobic and anaerobic conditions. Our data show that *V. cholerae* and *P. aeruginosa* CopI restore Cu resistance in *R. gelatinosus* under anaerobiosis, suggesting that in *V. cholerae* and *P. aeruginosa* CopI could be also required under oxygen limited conditions. With these conflicting data, we are pursuing further studies to elucidate the role of CopI/CopG system in these bacteria under anaerobiosis or microaerobiosis conditions.

Supporting Information: This article contains supporting information.

Acknowledgements:

ICP-MS experiments were performed in the MasSpecLab facility in Versailles Saint-Quentin-en-Yvelines University. Support from the EPR research network RENARD (FR-CNRS 3443) is gratefully acknowledged. We thank Emilien Etienne for assistance with the cw-EPR spectrometers and Yoshiharu Yamaichi for providing *Vibrio cholerae* strains. We thank Pascal Arnoux, Marianne Ilbert and Frédéric Biaso for fruitful discussions about this project. Pascal Arnoux, Solange Morera and Armelle Vigouroux are acknowledged for the crystallographic trials.

Conflict of Interest Statement: The authors declare that the study was conducted in the absence of any conflict of interest.

Data Availability Statement: The data underlying this article will be shared on reasonable request to the corresponding authors.

TABLE 1: **EPR parameters for the two Cu(II) sites in *Rg*CopI and related systems**

Protein and Cu(II) site	g_1	g_2	g_3	A_1/MHz	A_2/MHz	A_3/MHz	Ligands	Ref.
*Rg*CopI **T1.5**	2.199	2.062	2.019	207	41	143	2N, 2S	This work
AcoP **T1.5**	2.193	2.057	2.019	198	36	195	2N, 2S	[26]
NiR **T1.5** *A. faecalis*	2.195	2.055	2.025	236	-	-	2N, 2S	[39]
NiR **T1.5** *R. sphaeroides*	2.19	2.06	2.02	204	-	144	2N, 2S	[40]
Azurin **T1**	2.259	2.056	2.032	174	21	21	2N, 2S	[26]
*Rg*CopI **T2**	2.262	2.056	2.056	536	41	41	3N, 1O	This work
Cu($A\beta_{1-16}$) **T2**	2.263	2.057	2.057	539	50	50	3N, 1O	[42]
Cu(GHK) **T2**	2.23	2.05	2.05	560	-	-	3N, 1O	[46]
Cu(DAHK) **T2**	2.19	2.04	2.04	596	-	-	4N	[46]

REFERENCES

1. Palmer, L. D. & Skaar, E. P. (2016) Transition metals and virulence in bacteria, *Annu Rev Genet.* **50**, 67-91.

2. Checa, S. K., Giri, G. F., Espariz, M., Arguello, J. M. & Soncini, F. C. (2021) Copper Handling in the *Salmonella* Cell Envelope and Its Impact on Virulence, *Trends in microbiology.* **29**, 384-387.

3. Djoko, K. Y., Ong, C. L., Walker, M. J. & McEwan, A. G. (2015) The Role of Copper and Zinc toxicity in innate immune defense against bacterial pathogens, *J Biol Chem.* **290**, 18954-61.

4. White, C., Lee, J., Kambe, T., Fritsche, K. & Petris, M. J. (2009) A role for the ATP7A copper-transporting ATPase in macrophage bactericidal activity, *J Biol Chem.* **284**, 33949-56.

5. Crawford, C. L., Dalecki, A. G., Perez, M. D., Schaaf, K., Wolschendorf, F. & Kutsch, O. (2020) A copper-dependent compound restores ampicillin sensitivity in multidrug-resistant *Staphylococcus aureus*, *Scientific reports.* **10**, 8955.

6. Meir, A., Lepechkin-Zilbermintz, V., Kahremany, S., Schwerdtfeger, F., Gevorkyan-Airapetov, L., Munder, A., Viskind, O., Gruzman, A. & Ruthstein, S. (2019) Inhibiting the copper efflux system in microbes as a novel approach for developing antibiotics, *PLoS One.* **14**, e0227070.

7. Giachino, A. & Waldron, K. J. (2020) Copper tolerance in bacteria requires the activation of multiple accessory pathways, *Molecular microbiology.* **114**, 377-390.

8. Giner-Lamia, J., Lopez-Maury, L. & Florencio, F. J. (2014) Global transcriptional profiles of the copper responses in the cyanobacterium *Synechocystis* sp. PCC 6803, *PLoS One.* **9**, e108912.

9. Franke, S., Grass, G., Rensing, C. & Nies, D. H. (2003) Molecular analysis of the copper-transporting efflux system CusCFBA of *Escherichia coli*, *Journal of bacteriology.* **185**, 3804-12.

10. Pontel, L. B. & Soncini, F. C. (2009) Alternative periplasmic copper-resistance mechanisms in Gram negative bacteria, *Molecular microbiology.* **73**, 212-25.

11. Hausrath, A. C., Ramirez, N. A., Ly, A. T. & McEvoy, M. M. (2020) The bacterial copper resistance protein CopG contains a cysteine-bridged tetranuclear copper cluster, *J Biol Chem.* **295**, 11364-11376.

12. Elsen, S., Ragno, M. & Attree, I. (2011) PtrA is a periplasmic protein involved in Cu tolerance in *Pseudomonas aeruginosa*, *Journal of bacteriology.* **193**, 3376-8.

13. Teitzel, G. M., Geddie, A., De Long, S. K., Kirisits, M. J., Whiteley, M. & Parsek, M. R. (2006) Survival and growth in the presence of elevated copper: transcriptional profiling of copper-stressed *Pseudomonas aeruginosa*, *J Bacteriol.* **188**, 7242-56.

14. Quintana, J., Novoa-Aponte, L. & Arguello, J. M. (2017) Copper homeostasis networks in the bacterium *Pseudomonas aeruginosa*, *J Biol Chem.* **292**, 15691-15704.

15. Singh, S. K., Grass, G., Rensing, C. & Montfort, W. R. (2004) Cuprous oxidase activity of CueO from *Escherichia coli*, *Journal of bacteriology.* **186**, 7815-7.

16. Djoko, K. Y., Chong, L. X., Wedd, A. G. & Xiao, Z. (2010) Reaction mechanisms of the multicopper oxidase CueO from *Escherichia coli* support its functional role as a cuprous oxidase, *J Am Chem Soc.* **132**, 2005-15.

17. Outten, F. W., Huffman, D. L., Hale, J. A. & O'Halloran, T. V. (2001) The independent cue and cus systems confer copper tolerance during aerobic and anaerobic growth in *Escherichia coli*, *J Biol Chem.* **276**, 30670-7.

18. Quaranta, D., McCarty, R., Bandarian, V. & Rensing, C. (2007) The copper-inducible cin operon encodes an unusual methionine-rich azurin-like protein and a pre-Q0 reductase in *Pseudomonas putida* KT2440, *Journal of bacteriology.* **189**, 5361-71.

19. Marrero, K., Sanchez, A., Gonzalez, L. J., Ledon, T., Rodriguez-Ulloa, A., Castellanos-Serra, L., Perez, C. & Fando, R. (2012) Periplasmic proteins encoded by VCA0261-0260 and

VC2216 genes together with copA and cueR products are required for copper tolerance but not for virulence in *Vibrio cholerae*, *Microbiology.* **158**, 2005-2016.

20. Durand, A., Azzouzi, A., Bourbon, M. L., Steunou, A. S., Liotenberg, S., Maeshima, A., Astier, C., Argentini, M., Saito, S. & Ouchane, S. (2015) *c*-Type Cytochrome Assembly Is a Key Target of Copper Toxicity within the Bacterial Periplasm, *MBio.* **6**, e01007-15.

21. Selamoglu, N., Onder, O., Ozturk, Y., Khalfaoui-Hassani, B., Blaby-Haas, C. E., Garcia, B. A., Koch, H. G. & Daldal, F. (2020) Comparative differential cuproproteomes of *Rhodobacter capsulatus* reveal novel copper homeostasis related proteins, *Metallomics : integrated biometal science.* **12**, 572-591.

22. Wiethaus, J., Wildner, G. F. & Masepohl, B. (2006) The multicopper oxidase CutO confers copper tolerance to *Rhodobacter capsulatus*, *FEMS Microbiol Lett.* **256**, 67-74.

23. Wright, B. W., Kamath, K. S., Krisp, C. & Molloy, M. P. (2019) Proteome profiling of *Pseudomonas aeruginosa* PAO1 identifies novel responders to copper stress, *BMC microbiology.* **19**, 69.

24. Choi, M. & Davidson, V. L. (2011) Cupredoxins: a study of how proteins may evolve to use metals for bioenergetic processes, *Metallomics : integrated biometal science.* **3**, 140-51.

25. Perez-Henarejos, S. A., Alcaraz, L. A. & Donaire, A. (2015) Blue Copper Proteins: A rigid machine for efficient electron transfer, a flexible device for metal uptake, *Arch Biochem Biophys.* **584**, 134-48.

26. Roger, M., Biaso, F., Castelle, C. J., Bauzan, M., Chaspoul, F., Lojou, E., Sciara, G., Caffarri, S., Giudici-Orticoni, M. T. & Ilbert, M. (2014) Spectroscopic characterization of a green copper site in a single-domain cupredoxin, *PLoS One.* **9**, e98941.

27. King, J. D., McIntosh, C. L., Halsey, C. M., Lada, B. M., Niedzwiedzki, D. M., Cooley, J. W. & Blankenship, R. E. (2013) Metalloproteins diversified: the auracyanins are a family of cupredoxins that stretch the spectral and redox limits of blue copper proteins, *Biochemistry.* **52**, 8267-75.

28. Suzuki, K., Kataoka, K., Yamaguchi, K., Inoue, T. & Kai, Y. (1999) Structure-function relationships of copper-containing nitrite reductases., *Coord Chem Rev.* **190-192**, 245-265.

29. Arciero, D. M., Pierce, B. S., Hendrich, M. P. & Hooper, A. B. (2002) Nitrosocyanin, a red cupredoxin-like protein from *Nitrosomonas europaea*, *Biochemistry.* **41**, 1703-9.

30. Sambrook, J., Fritsch, E. & Maniatis, T. (1989) *Molecular cloning, a laboratory manual*, 2nd edition edn, New York,

NY: Cold Spring Harbor.

31. Ouchane, S., Picaud, M., Reiss-Husson, F., Vernotte, C. & Astier, C. (1996) Development of gene transfer methods for *Rubrivivax gelatinosus* S1: construction, characterization and complementation of a puf operon deletion strain, *Mol Gen Genet.* **252**, 379-85.

32. Haan, C. & Behrmann, I. (2007) A cost effective non-commercial ECL-solution for Western blot detections yielding strong signals and low background, *Journal of Immunological Methods.* **318**, 11-19.

33. Ybe, J. A. & Hecht, M. H. (1994) Periplasmic fractionation of *Escherichia coli* yields recombinant plastocyanin despite the absence of a signal sequence, *Protein expression and purification.* **5**, 317-23.

34. Stoll, S. & Schweiger, A. (2006) EasySpin, a comprehensive software package for spectral simulation and analysis in EPR, *Journal of Magnetic Resonance.* **178**, 42-55.

35. Correia dos Santos, M., Paes de Sousa, P. M., Simões Gonçalves, M. L., Krippahl, L., Moura, J. J. G., Lojou, E. & Bianco, P. (2003) Electrochemical studies on small electron transfer proteins using membrane electrodes, *J Electroanal Chem.* **541**, 153–162.

36. Vanhove, A. S., Rubio, T. P., Nguyen, A. N., Lemire, A., Roche, D., Nicod, J., Vergnes, A., Poirier, A. C., Disconzi, E., Bachere, E., Le Roux, F., Jacq, A., Charriere, G. M. & Destoumieux-Garzon, D. (2016) Copper homeostasis at the host vibrio interface: lessons from intracellular vibrio transcriptomics, *Environ Microbiol.* **18**, 875-88.

37. Solomon, E. I. (2006) Spectroscopic methods in bioinorganic chemistry: blue to green to red copper sites, *Inorganic chemistry.* **45**, 8012-25.

38. Peisach, J. & Blumberg, W. E. (1974) Structural implications derived from the analysis of electron paramagnetic resonance spectra of natural and artificial copper proteins, *Arch Biochem Biophys.* **165**, 691-708.

39. Fittipaldi, M., Wijma, H. J., Verbeet, M. P., Canters, G. W. & Huber, M. (2006) Electronic structure of the two copper sites in nitrite reductase by 9 and 95 GHz EPR on cavity mutants, *Applied Magnetic Resonance.* **30**, 417.

40. Olesen, K., Veselov, A., Zhao, Y., Wang, Y., Danner, B., Scholes, C. P. & Shapleigh, J. P. (1998) Spectroscopic, kinetic, and electrochemical characterization of heterologously expressed wild-type and mutant forms of copper-containing nitrite reductase from *Rhodobacter sphaeroides* 2.4.3, *Biochemistry.* **37**, 6086-94.

41. Kukimoto, M., Nishiyama, M., Murphy, M. E., Turley, S., Adman, E. T., Horinouchi, S. & Beppu, T. (1994) X-ray structure and site-directed mutagenesis of a nitrite reductase from *Alcaligenes faecalis* S-6: roles of two copper atoms in nitrite reduction, *Biochemistry.* **33**, 5246-52.

42. Dorlet, P., Gambarelli, S., Faller, P. & Hureau, C. (2009) Pulse EPR spectroscopy reveals the coordination sphere of copper(II) ions in the 1-16 amyloid-beta peptide: a key role of the first two N-terminus residues, *Angewandte Chemie International Edition.* **48**, 9273-9276.

43. Roberts, S. A., Weichsel, A., Grass, G., Thakali, K., Hazzard, J. T., Tollin, G., Rensing, C. & Montfort, W. R. (2002) Crystal structure and electron transfer kinetics of CueO, a multicopper oxidase required for copper homeostasis in *Escherichia coli*, *Proc Natl Acad Sci U S A.* **99**, 2766-71.

44. Yang, D., Klebl, D. P., Zeng, S., Sobott, F., Prevost, M., Soumillion, P., Vandenbussche, G. & Fontaine, V. (2020) Interplays between copper and *Mycobacterium tuberculosis* GroEL1, *Metallomics : integrated biometal science.* **12**, 1267-1277.

45. Ansari, M. Y., Batra, S. D., Ojha, H., Dhiman, K., Ganguly, A., Tyagi, J. S. & Mande, S. C. (2020) A novel function of *Mycobacterium tuberculosis* chaperonin paralog GroEL1 in copper homeostasis, *FEBS letters*.

46. Hureau, C., Eury, H., Guillot, R., Bijani, C., Sayen, S., Solari, P. L., Guillon, E., Faller, P. & Dorlet, P. (2011) X-ray and solution structures of Cu(II) GHK and Cu(II) DAHK complexes: influence on their redox properties, *Chemistry.* **17**, 10151-60.

47. Steunou, A. S., Babot, M., Bourbon, M. L., Tambosi, R., Durand, A., Liotenberg, S., Krieger-Liszkay, A., Yamaichi, Y. & Ouchane, S. (2020) Additive effects of metal excess and superoxide, a highly toxic mixture in bacteria, *Microbial biotechnology.* **13**, 1515-1529.

A

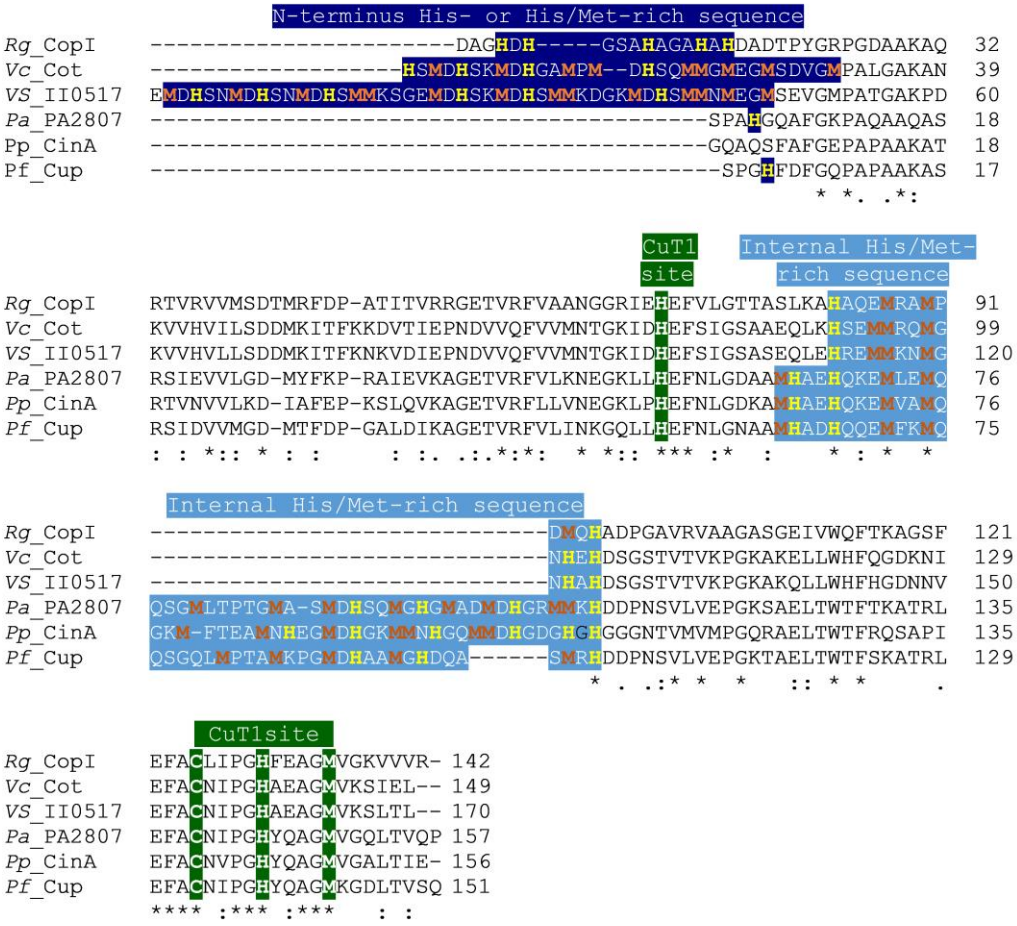

B

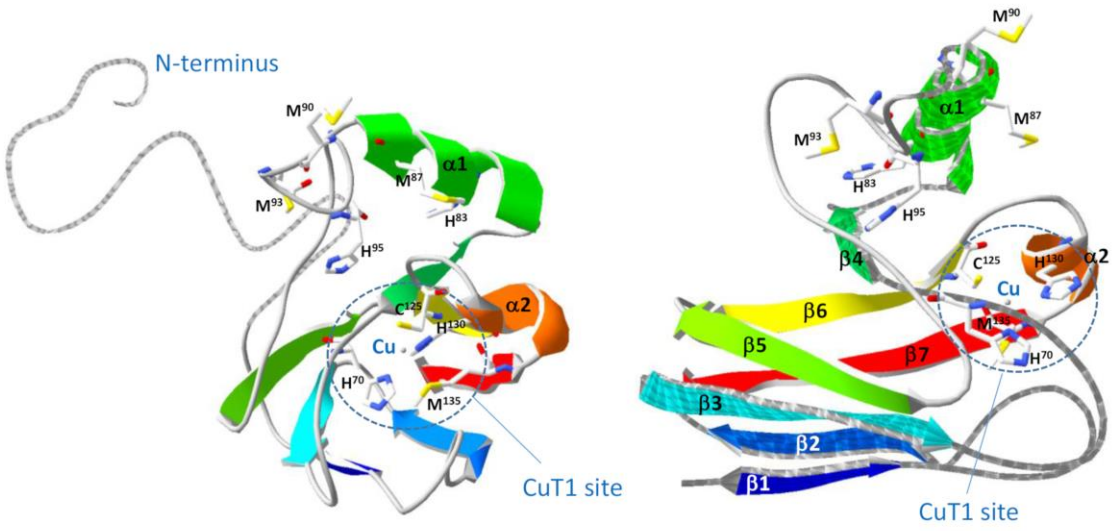

Figure 1: Sequence alignments of various putative bacterial CopI proteins and homology modelling of *R. gelatinosus* CopI. (A) Mature sequences of *R. gelatinosus* CopI (*Rg_CopI*), *V.*

cholerae (*Vc*_Cot), *V. tasmaniensis* LGP 32 (VS_II0517), *P. aeruginosa* PAO1 (*Pa*_PA2807), *Pseudomonas putida* CinA (*Pp*_CinA) WP_010953146 and *Pseudomonas fluorescens* (*Pf*_Cup) WP_060738394.1 are indicated. Three remarkable sequences were reported: (i) the four residues of the putative CuT1 site are in bold and highlighted in dark green (His^{70} Cys^{125} His^{130} Met^{135} for *R. gelatinosus* CopI numbering); (ii) the N-terminus His-rich or His/Met-rich sequence is highlighted in dark blue, with histidines and methionines in yellow and brown respectively; (iii) the internal His/Met-rich sequence is highlighted in light blue, with histidines and methionines in yellow and brown respectively. Sequence alignment was performed with ClustalW; identical (*), strongly similar (:) and weakly similar (.) amino acids are indicated. (B) Homology modelling of *R. gelatinosus* CopI using the various cupredoxin structures as templates. Two views of the proteins are represented. On the right panel, the unfolded N-terminus is not represented and the model starts at Thr^{34} for clarity. The Cu atom (grey ball stick), the lateral chains of His^{70}, His^{130}, Cys^{125} and Met^{135} of the CuT1 site and of histidines and methionines of the internal His/Met-rich sequence are displayed. The β strands and α helices are colored. This model was generated by Modeller and the images created using Swiss-PDB viewer.

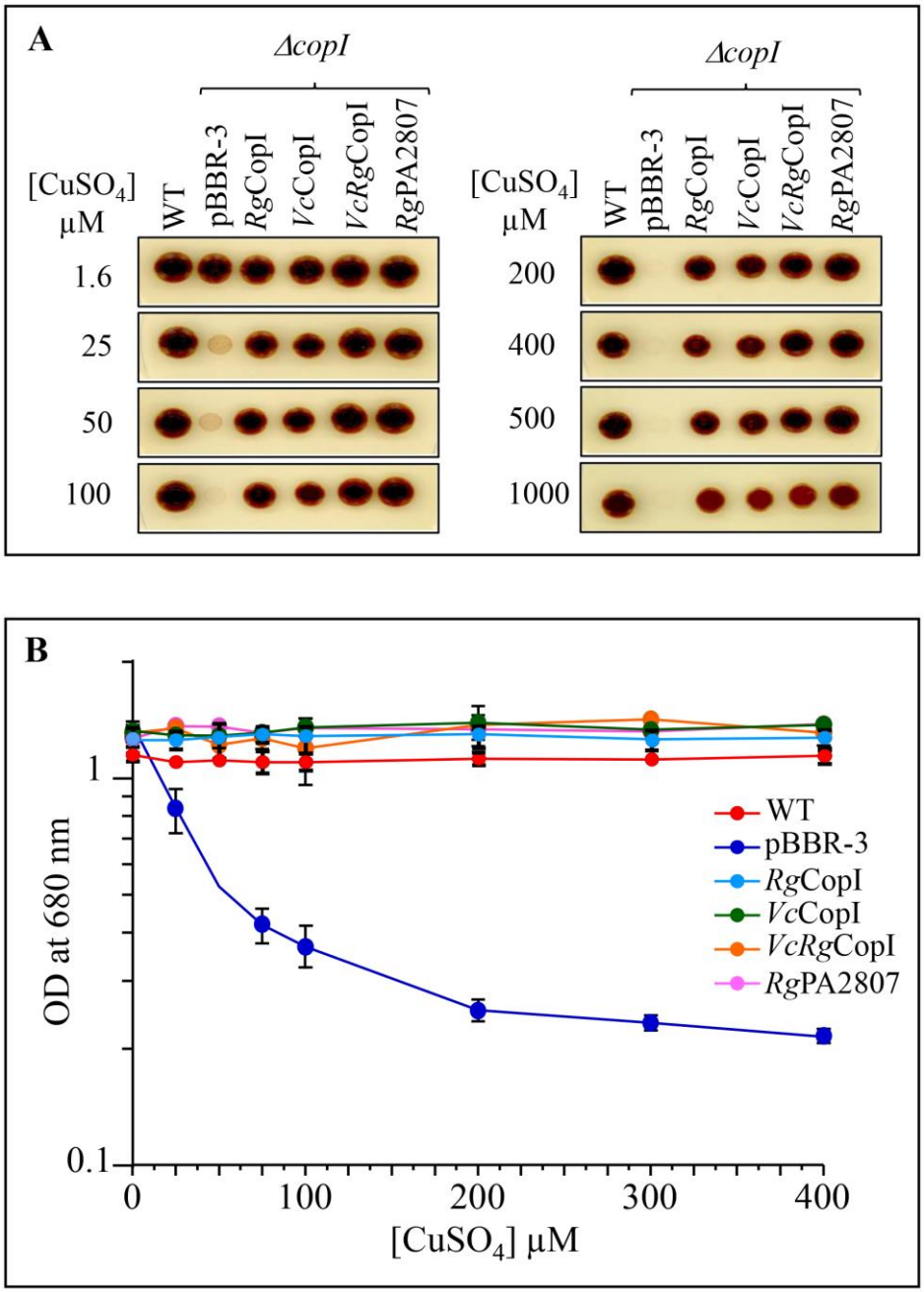

Figure 2: *V. cholerae* and *P. aeruginosa* CopI homologues protect *R. gelatinosus ΔcopI* mutant from Cu toxicity. (A) Growth phenotype of the WT *R. gelatinosus*, *ΔcopI* mutant complemented with WT *V. cholerae* CopI (*Vc*CopI), *P. aeruginosa* PA2807 (*Rg*PA2807) with the added N-terminus His-rich of *Rg*CopI or the *VcRg*CopI chimera expressing *Rg*CopI with the *Rg* His-rich N-terminus substituted for the His/Met-rich N-terminus of *V. cholerae* CopI. *ΔcopI* mutant complemented with pBBR-3 or *R. gelatinosus* WT CopI (*Rg*CopI) were used as negative and positive control respectively. Strains, overnight grown under photosynthesis (PS) conditions, were spotted (3 µL of 1 $OD^{680\ nm}$ culture) on solid malate medium supplemented

with increasing $CuSO_4$ concentrations. Plates were incubated under PS for 24 h at 30°C prior to photography. (B) Growth inhibition of the same strains challenged with increasing $CuSO_4$ concentrations under PS conditions. Cells were grown for 24 h at 30°C before optical density (OD) measurement at 680 nm. The error bars represent the standard deviation of the mean of three independent experiments.

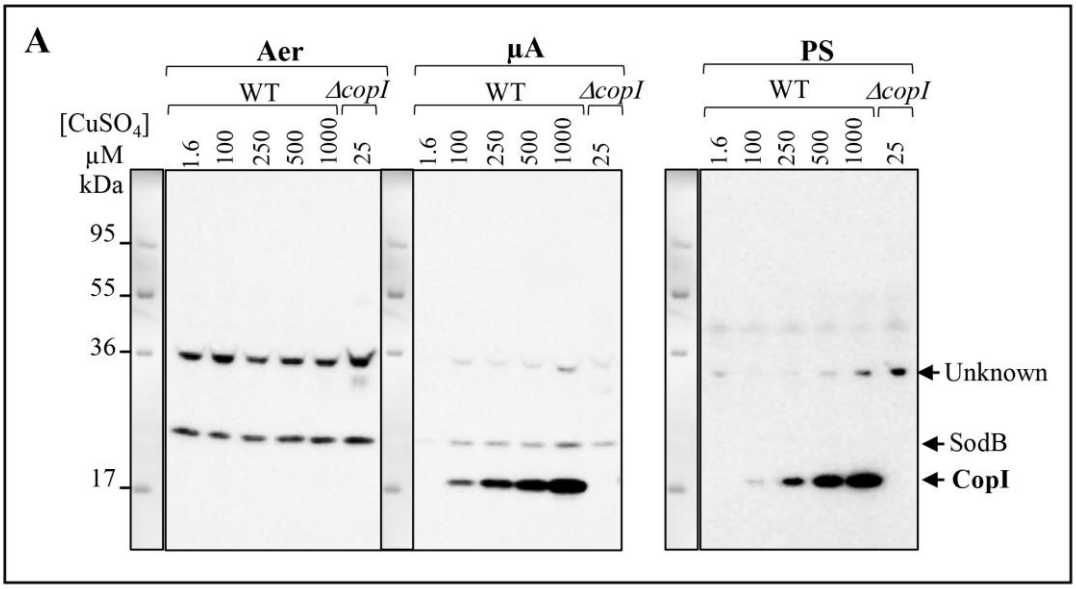

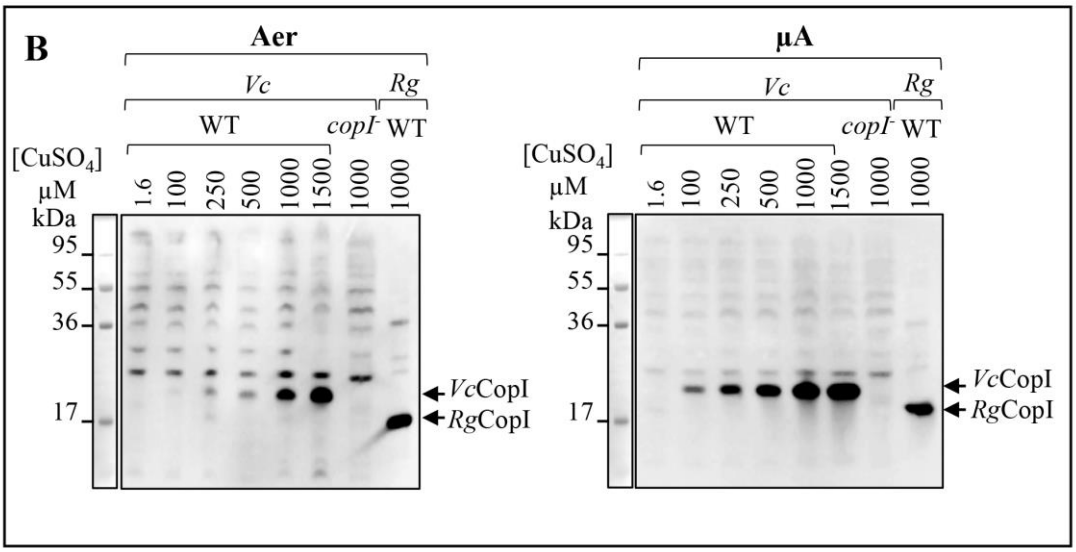

Figure 3: The Cu-inducible expression of CopI is higher under low oxygen concentration both in *R. gelatinosus* and *V. cholerae*. (A) Expression level of CopI in *R. gelatinosus* wild-type (WT) cells challenged with increasing $CuSO_4$ concentrations, *ΔcopI* mutant cells grown in the presence of 25 µM $CuSO_4$ were used as negative control. Cells were grown in malate medium overnight (18 h) under aerobic (Aer), microaerobic (µAer) and photosynthetic (PS) conditions. The SodB expression is indicated [47]. (B) Expression level of CopI in *V. cholerae* wild-type (WT) cells challenged with increasing $CuSO_4$ concentrations. Cells were grown in LB

medium overnight (18 h) under aerobic (Aer) and microaerobic (µAer) conditions. VC-A0620::Tn strain, deleted for *copI* gene, was grown under aerobiosis in the presence of 1 mM $CuSO_4$ and used as negative control. *R. gelatinosus* WT (*Rg* WT) cells grown under microaerobic conditions in the presence of $CuSO_4$ in malate medium were added for comparison. The *V. cholerae Vc*CopI and the *R. gelatinosus Rg*CopI proteins are indicated. For all the gels showed, total protein extract from the same amount of cells (OD^{680nm} = 0.1) were separated on a 15% Tris-glycine SDS-PAGE. Proteins were visualized after Western blotting using the HRP-HisProbe.

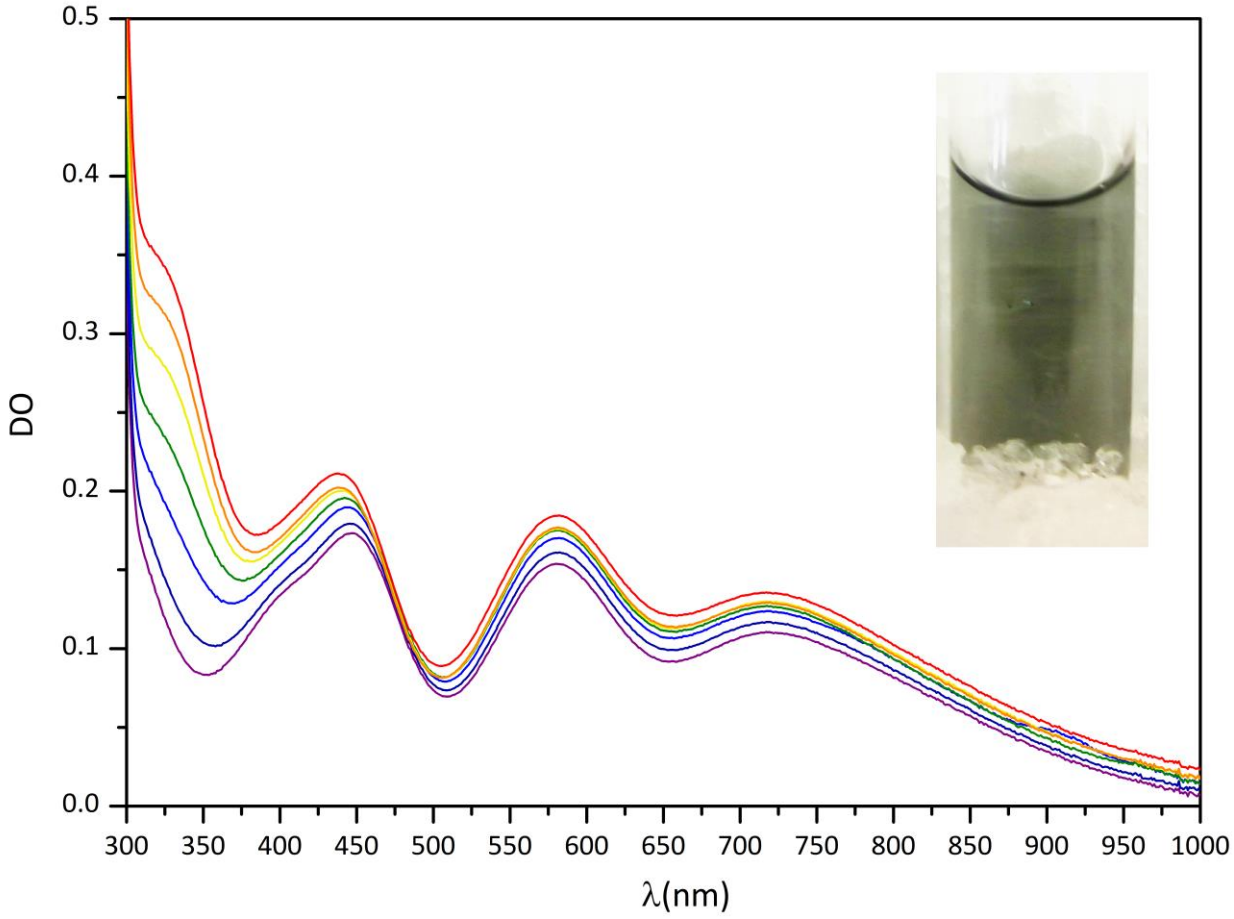

Figure 4: UV-visible titration of pure *R. gelatinosus* CopI by addition of Cu(II). The spectrum of the purified protein (150 µM) is shown as purple line (lowest intensity spectrum). Other spectra correspond to the addition of Cu(II) (50 µM indigo, 100 µM blue, 150 µM green, 200 µM yellow, 250 µM orange, 300 µM red). Inset: image of the pure *Rg*CopI solution eluted from the S200.

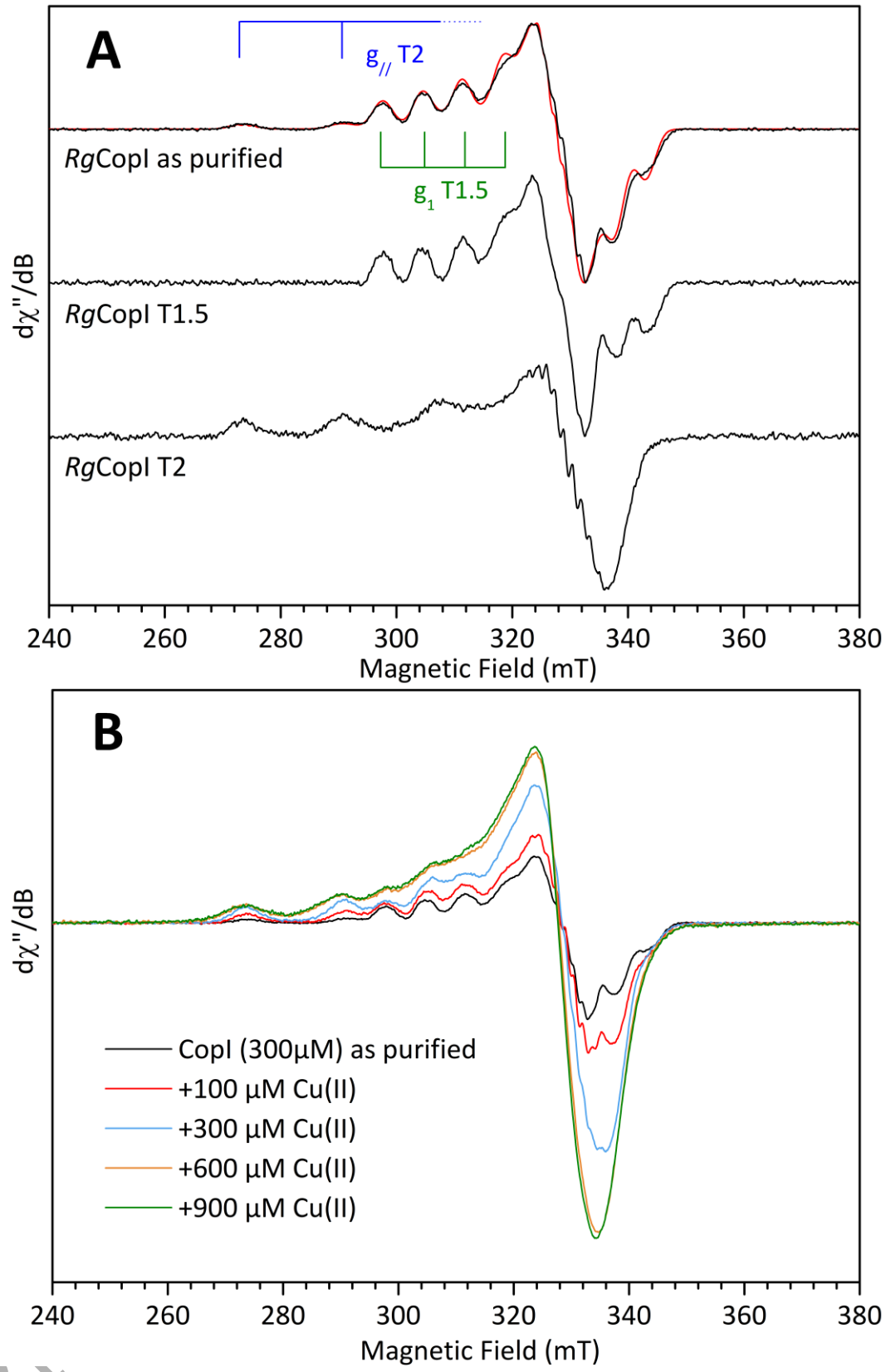

Figure 5: EPR spectrum of pure *R. gelatinosus* CopI and Cu(II) titration. (A) EPR spectrum of pure *R. gelatinosus* CopI (top spectrum, black line) along its simulation (red line) and EPR signatures of the two contributions from the T1.5 and T2 sites. The contributions were

isolated by linear combinations of spectra presented in panel B. (B) Cu(II) titration of *Rg*CopI followed by EPR. Experimental conditions: microwave frequency 9.48 GHZ, microwave power 1mW, modulation amplitude 0.5 mT, T 100 K, protein concentration 300 µM.

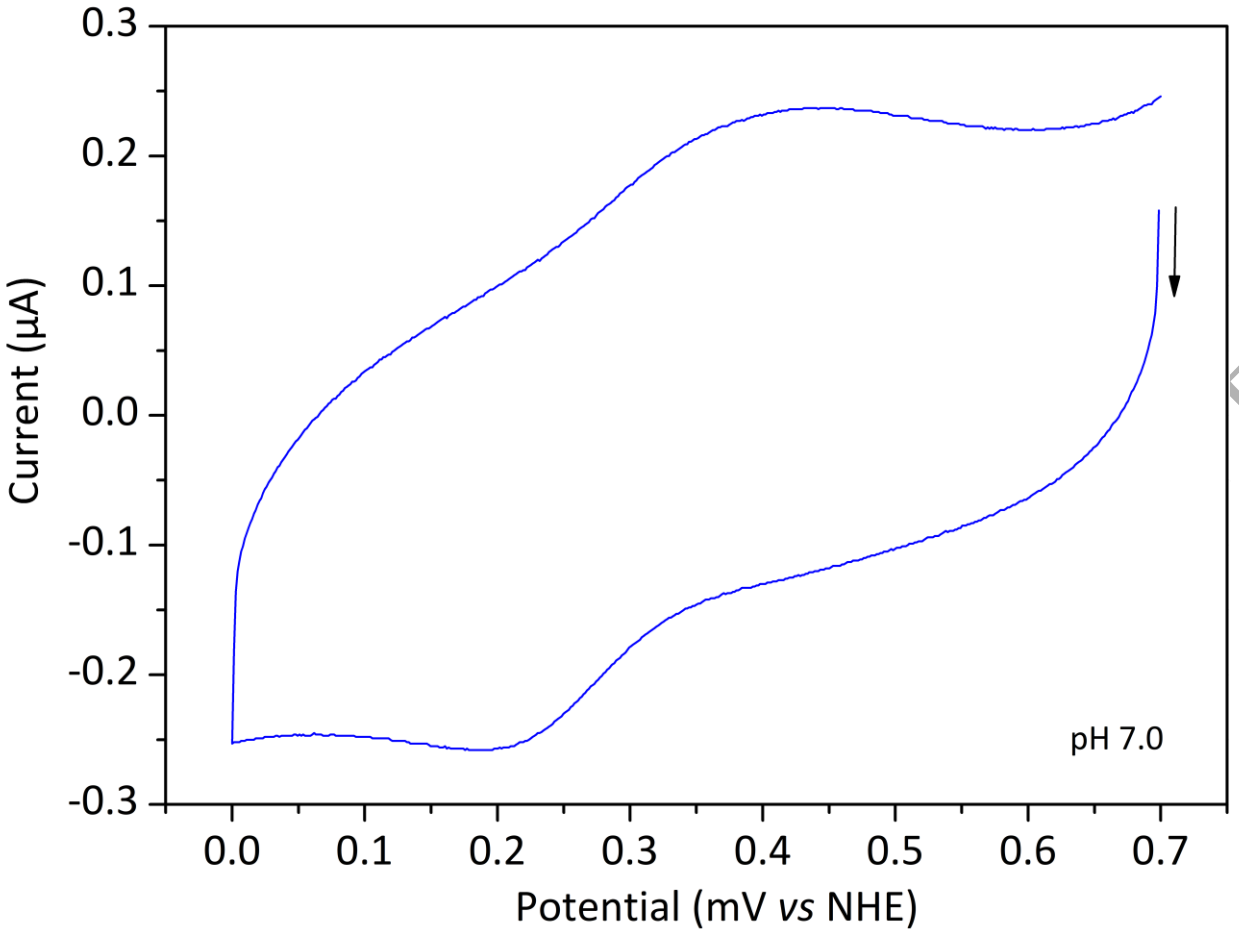

Figure 6: **Cyclovoltamogramm of pure *R. gelatinosus* CopI at pH 7.0**. Cyclic voltammetry experiments recorded at a pyrolytic graphite electrode with 2 µM of *Rg* CopI embedded between the surface of the electrode and a dialysis membrane in a thin layer configuration. Bis-tris 50 mM buffer pH 7, sweep rate 20 mV s^{-1}.

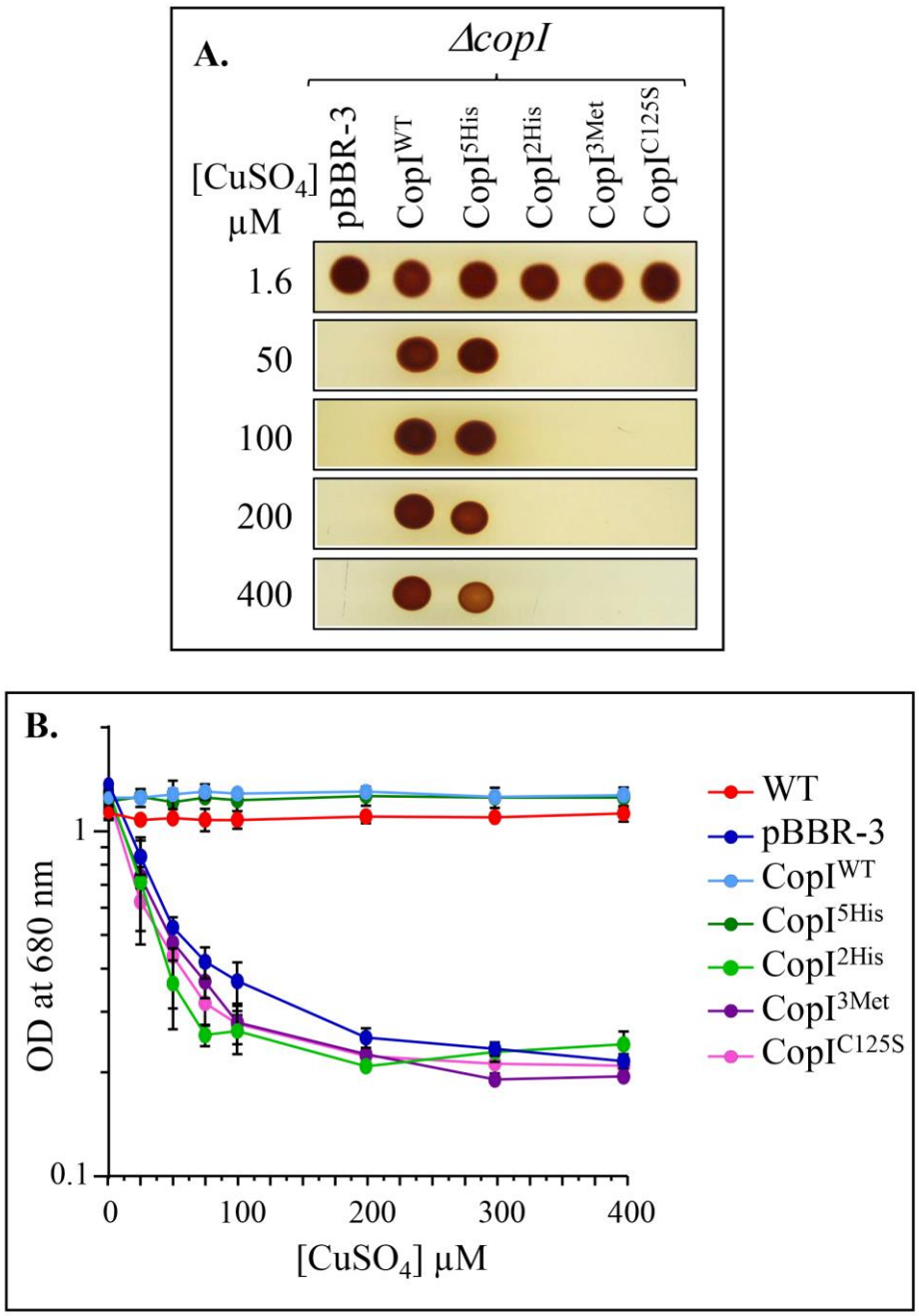

Figure 7: Characterization of *R. gelatinosus* CopI mutants. (A) Growth phenotype of the *R. gelatinosus ΔcopI* mutant complemented with WT or various *R. gelatinosus* CopI mutants on solid malate medium supplemented with $CuSO_4$. Strains complemented with pBBR-3 or *R. gelatinosus* WT CopI ($CopI^{WT}$) were used as negative and positive controls respectively. Strains (overnight grown under PS conditions) were spotted (3 µL of the same amount of cells: OD^{680nm} = 1)) on solid malate medium supplemented with increasing $CuSO_4$ concentrations. Plates were incubated under photosynthesis (PS) for 24 h at 30°C prior to photography. (B) Growth inhibition of the WT and *ΔcopI* mutant complemented with WT or various CopI mutants

challenged with increasing $CuSO_4$ concentrations under photosynthesis conditions. Cells were grown for 24 h at 30°C before OD at 680 nm measurement. The error bars represent the standard deviation of the mean of three independent experiments.

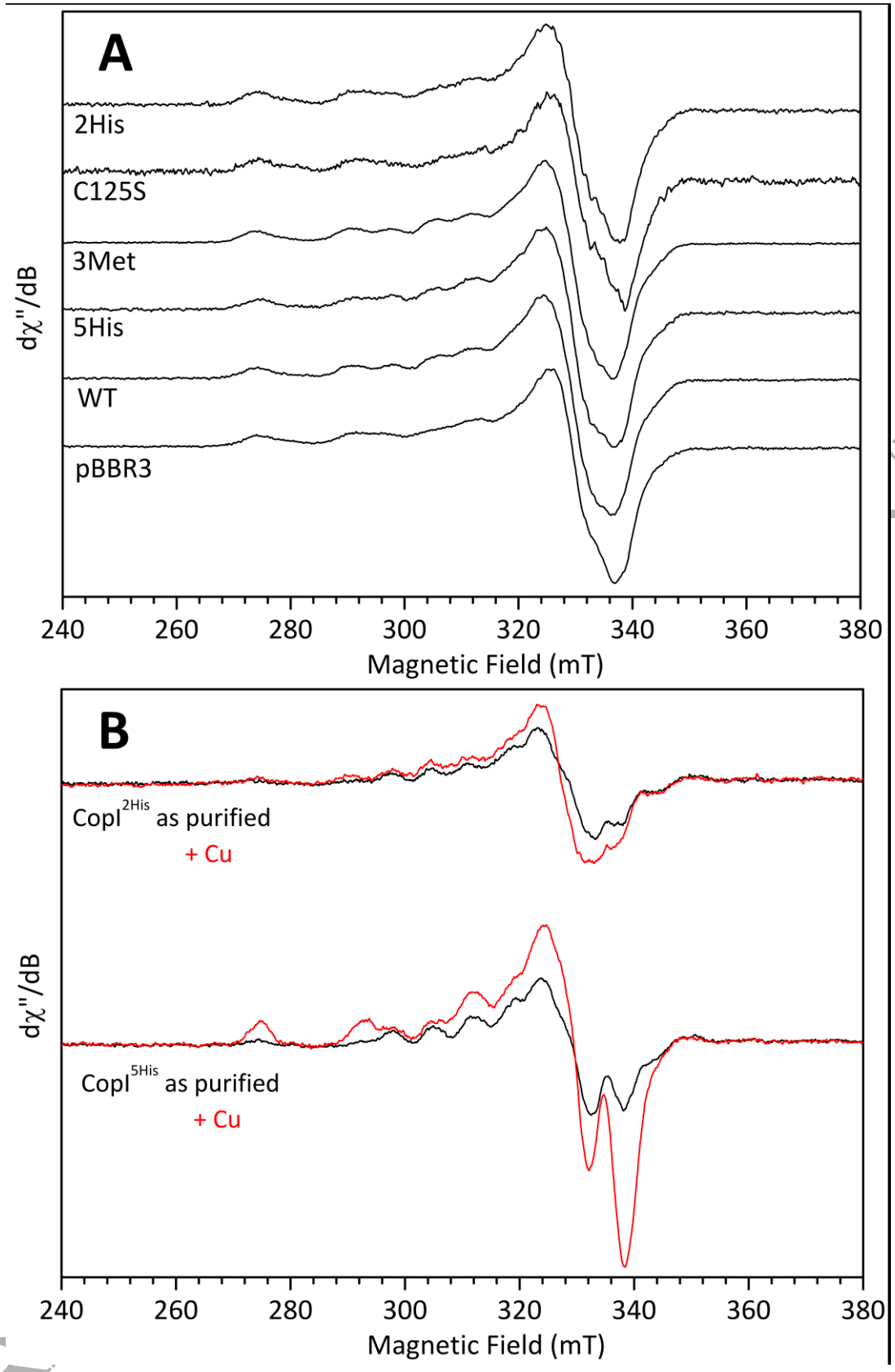

Figure 8: EPR spectra of *R. gelatinosus* CopI mutants. (A) EPR spectra of the soluble fractions of *Rg*CopI mutants. Experimental conditions: microwave frequency 9.48 GHZ,

microwave power 1mW, modulation amplitude 0.5 mT, T 100 K. Spectra have been scaled for clarity. (B) X-band EPR spectra of the two purified mutants $CopI^{2His}$ and $CopI^{5His}$ before (black lines) and after (red lines) addition of 0.8-0.9 equivalent of Cu(II). Experimental conditions: microwave frequency 9.48 GHZ, microwave power 1mW, modulation amplitude 1 mT, T 100 K, proteins concentration 20 µM ($CopI^{2His}$) and 45 µM ($CopI^{5His}$).